Original article

Institution of MECHANICAL ENGINEERS
Journal of MATERIALS: DESIGN AND APPLICATIONS

Proc IMechE Part L:
J Materials: Design and Applications
2016, Vol. 230(3) 748–759

DOI: 10.1177/1464420714566629
pil.sagepub.com
SAGE

Study of the deep drawing behavior and crystallographic texture of AA 3104-H19 aluminum alloy sheets

André LT Martins[1], Antônio A Couto[1,2] and Nelson B Lima[2]

Abstract

The aluminum alloy 3104, H19 temper, is commonly used in the production of two-piece beverage cans. The objective of the present study is to compare three different rolled sheets of this alloy. All three of them are routinely used in production lines dedicated to can manufacturing. The yield strength for all three was found around 265 MPa, the ultimate tensile strength 281 MPa, and the average elongation 4.19%. The strain hardening exponent (n) was similar for all three sheets, averaging 0.078. The plastic strain ratios for planar anisotropy (ΔR) and for normal anisotropy ($\overline{R}$) were found to be near zero and 0.4, respectively. Values of ΔR near zero indicate there is no earing tendency. The crystallographic texture analysis yielded four dominating components: Brass ({110}<112>) and Copper ({112}<111>), which are typical of strain hardened aluminum, Cube ({001}<100>), usually associated with recrystallization, and Goss ({110}<001>). Such a texture would be conducive to balanced earing. The metallographic images for all three sheets were alike, with constituents not homogeneously distributed and with similar size and chemical compositions in addition to dispersoids finely spread throughout the aluminum matrix. The Erichsen tests also showed alike results with an average of 4.6 mm before failure.

Keywords

Aluminum Alloy 3104, mechanical properties, crystallographic texture, strain hardening exponent, plastic strain ratios

Date received: 27 August 2014; accepted: 8 December 2014

Introduction

Aluminum alloys of the 3XXX series have as their main alloying element manganese (Mn). The addition of Mn to aluminum as a way of increasing its mechanical properties without compromising its corrosion resistance dates back to 1906. The aluminum alloy designated 3003 had 1.25% Mn and 0.12% Cu in its chemical composition and its early use was found in photographic cameras.[1] The 3004 alloy, a precursor alloy of the material used in the present study, had 1% Mg added to its composition to improve its strain hardening capacity, and it is still used currently in some two-piece beverage can plants. Because of its mechanical and corrosion resistance, these alloys were chosen as the material of choice for can manufacturing and that is the reason why they are among the high-volume aluminum alloys produced today.[1]

In order to reach the necessary mechanical properties, the alloy 3104 is cold rolled to the H19 temper, a process which not only alters the strength of the material by increasing its dislocation density but also changes its crystallographic texture components and intensities.[2] The properties of the finished product, a coil with specific width, length, and thickness, are known to influence the draw and wall ironing (DWI) process performance.[3] Another important factor in the DWI process is the earing tendency of the material which is related to its naturally occurring anisotropy and is exacerbated or made subtle by its crystallographic texture, many times influenced by the thermomechanical processes the material goes through.[4]

Aiming to better understand the properties of the alloy, a comparative characterization between three different rolled sheets extracted from coils used in the manufacturing process was undertaken. The mechanical properties were acquired by uniaxial tensile tests, Erichsen tests, and microhardness (Vickers) tests. With the data gathered in the tensile tests, the strain hardening exponent (n), the planar anisotropy (ΔR), and the normal anisotropy ($\overline{R}$) were calculated.

[1]Engineering Department, Mackenzie Presbyterian University, Brazil
[2]Materials Science and Technology Center, Nuclear and Energy Research Institute, Brazil

Corresponding author:
Antônio A Couto, Materials Science and Technology Center, Nuclear and Energy Research Institute, Cidade Universitária, São Paulo 05508-000, Brazil.
Email: acouto@ipen.br

The use of both optical and scanning electron microscopes (SEM) allowed for metallographic images to be acquired in addition to qualitative chemical composition of the alloy and its intermetallic compounds by the use of energy dispersion spectrometry (EDS). Crystallographic textures were obtained by the use of an automatic goniometer attached to a diffractometer.

Surface roughness tests (R_a) were also carried out. Finally, the results obtained for the three sheets were compared in search of similarities or discrepancies, which could in the future be correlated with production line performance. A secondary objective of the present work is to bring together information about the alloy 3104 H19, also commonly called can body stock (CBS), since much research has been dedicated to this material and comparison values are often useful.

Materials and methods

For the present study, three rolled sheets of aluminum alloy AA 3104 H19 were utilized. Two of them, hereafter designated S_{II} and S_{IV} were produced nationally and had different production routes after the tandem mill. S_{II} went through a single-stage cold mill and for that reason had to have multiples passes to reach its final gauge. S_{IV} went through a more modern multiple stage cold mill and one operation sufficed the necessary reductions for the specified gauge. The production route of a direct chill cast ingot that is laminated to the final gauge can be seen in Figure 1. The two different routes undertaken by S_{II} and S_{IV} can also be seen in the same figure.

The third sheet, designated S_{VI}, was from abroad and its fabrication details are unknown. All sheets had 0.270 mm as their final gauge and were extracted from the beginning of the coils. The other coil dimensions vary according to the die sets used and the weight capacity of the uncoiler. The most modern presses already have sets containing 15 dies, which take the coil width to approximately 1.79 m. The length will be established by the weight capacity of the equipment responsible to feed the material into the press, it is not uncommon to have coils weighting around 12 tonnes with lengths that reach around 10 km. Table 1 shows the different materials used and the nomenclature adopted for the present work.

Although the tolerances for Mn in the 3104 alloy composition vary from 0.8% to 1.4%, many times the amount of Magnesium exceeds that of Mn.[5] Different sources mention Mg as an element that promotes hardening by cold work more efficiently than Mn in aluminum alloys.[1,6] Table 2 shows the standard chemical composition of the aluminum alloy 3104 according to the American Society for Materials (ASM) and those for S_{II} and S_{IV} as informed by the supplier.[7] The chemical composition of S_{VI} was not informed.

The uniaxial tensile tests were realized with specimens cut out of the sheets at 0°, 45°, and 90° in relation to the rolling direction (RD). For each direction, four specimens were tested, making a total of 36 tests for the three different sheets. The dimensions of the specimens followed the Brazilian standard NBR 7549 and can be seen in Figure 2. The method used for extracting the specimens from the sheets was laser cut, Figure 3 shows S_{II} as an example. Figures 4 and 5, respectively, show the entry and exit points

Table 1. Materials and nomenclature used in the present study.

Nomenclature	Sheet	Cold Mill	Alloy	Temper
S_{II}	Rolled sheet II	Single stand	3104	H19
S_{IV}	Rolled sheet IV	Multiple stand	3104	H19
S_{VI}	Rolled sheet VI	Unknown	3104	H19

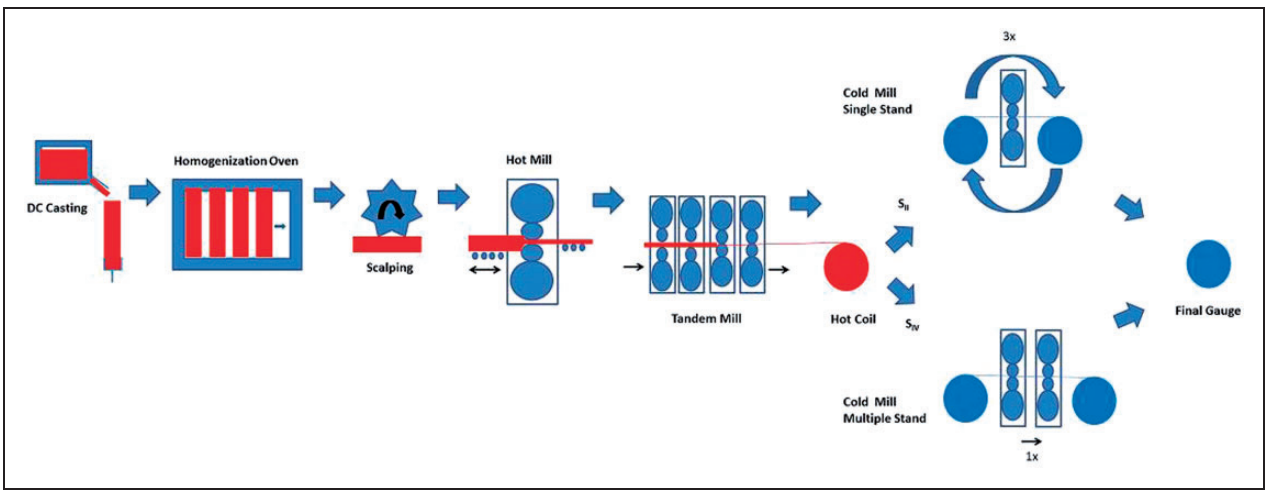

Figure 1. Production routes for sheet II and IV. DC: direct chill.

Table 2. Standard chemical composition of AA 3104 aluminum alloy according to the ASM and those for S_{II} and S_{IV}.

Source	Alloy	Si	Fe	Cu	Mn	Mg	Zn	Ti	Ga	V
$ASM_{Vol\ 2}$	3104	0.6	0.8	0.05–0.25	0.8–1.4	0.8–1.3	0.25	0.1	0.05	0.05
S_{II}	3104	0.19	0.5	0.10–0.18	0.80–0.90	1.10–1.20	0.05	0.015	N/I	N/I
S_{IV}	3104	0.19	0.5	0.10–0.18	0.80–0.90	1.10–1.20	0.04	0.014	N/I	N/I
S_{VI}	3104	N/I	N/I	N/I	N/I	N/I	N/I	N/I	N/I	N/I

ASM: American Society for Materials; N/I: not informed.

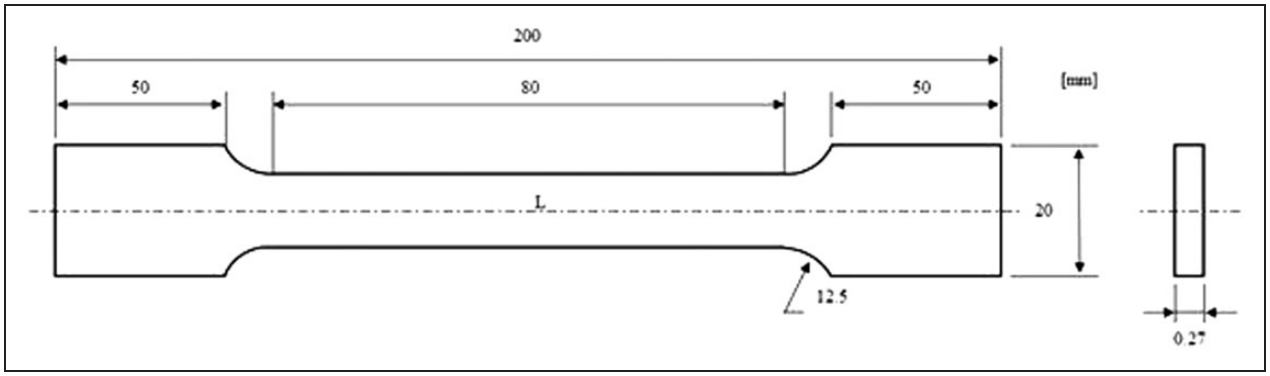

Figure 2. The dimentions of the specimens used for tensile tests.

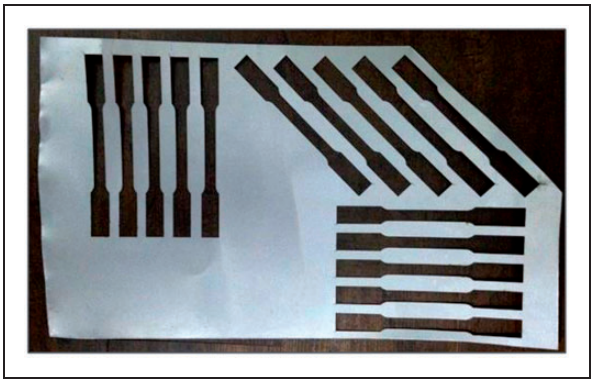

Figure 3. Laser cut extraction method of specimens for tensile tests.

of the laser beam in the sheet and a drawing of the laser cut system.

The results obtained from the tensile tests were the yield strength, the ultimate tensile strength, and the percent elongations. In order to obtain the strain hardening exponent n for each of the specimens, the data from the engineering curve had to be transformed in to the true stress and true strain curve. The true stress and strain values were calculated by equations (1) and (2). The norm SEW 1125, seen in equation (3), was used for the individual values of n.[8] The data used to calculate n considered only the plastic portion of the engineering curve up to the maximum stress value.

$$\sigma = \mathbf{s}(1 + \mathbf{e}) \tag{1}$$

$$\boldsymbol{\varepsilon} = \mathbf{ln}(1 + \mathbf{e}) \tag{2}$$

$$n = \frac{N\sum_{i=1}^{N}(\ln(\varepsilon)*\ln(\sigma)) - \left(\sum_{i=1}^{N}\ln(\varepsilon)\right)*\left(\sum_{i=1}^{N}\ln(\sigma)\right)}{N\sum_{I=1}^{N}(\ln(\varepsilon))^2 - \left(\sum_{i=1}^{N}\ln(\varepsilon)\right)^2} \tag{3}$$

where:

n	strain hardening exponent
N	sample number
σ	true stress
ε	true strain
s	engineering stress
e	engineering strain

The plastic strain ratios or Lankford values (R), normal anisotropy $\overline{R}$, and planar anisotropy ΔR were calculated using equations (4) to (6). The test specimens were measured at 16 mm intervals and the average of the five points was used as the final width (W_f) in the equations.

$$R = \frac{\varepsilon_w}{\varepsilon_t} = -\frac{\varepsilon_w}{\varepsilon_w + \varepsilon_l} = \frac{\ln\left(\frac{W_o}{W_f}\right)}{\ln\left(\frac{L_f * W_f}{L_o * W_o}\right)} \tag{4}$$

$$\overline{R} = \frac{R_0 + 2R_{45} + R_{90}}{4} \tag{5}$$

$$\Delta R = \frac{R_0 - 2R_{45} + R_{90}}{2} \tag{6}$$

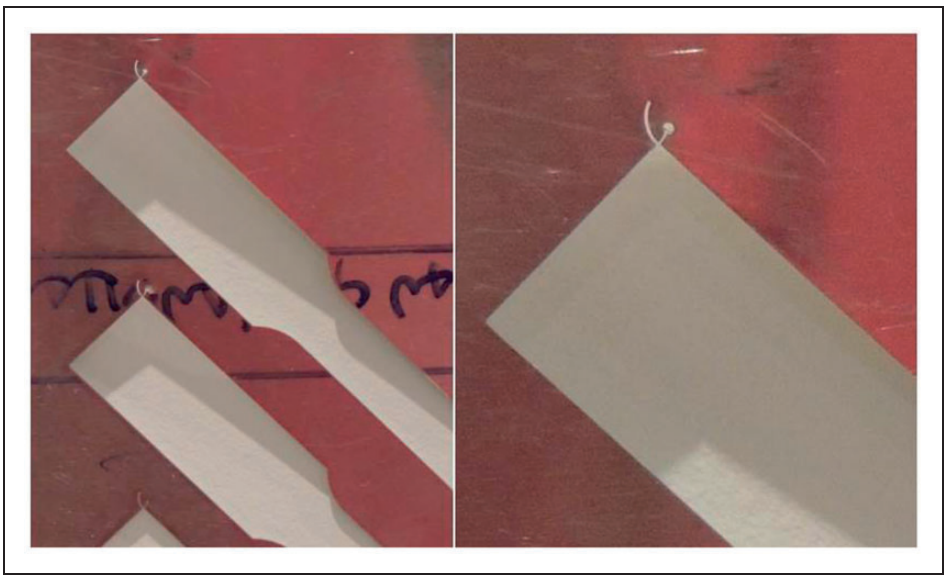

Figure 4. Entry point of laser beam and exit curve.

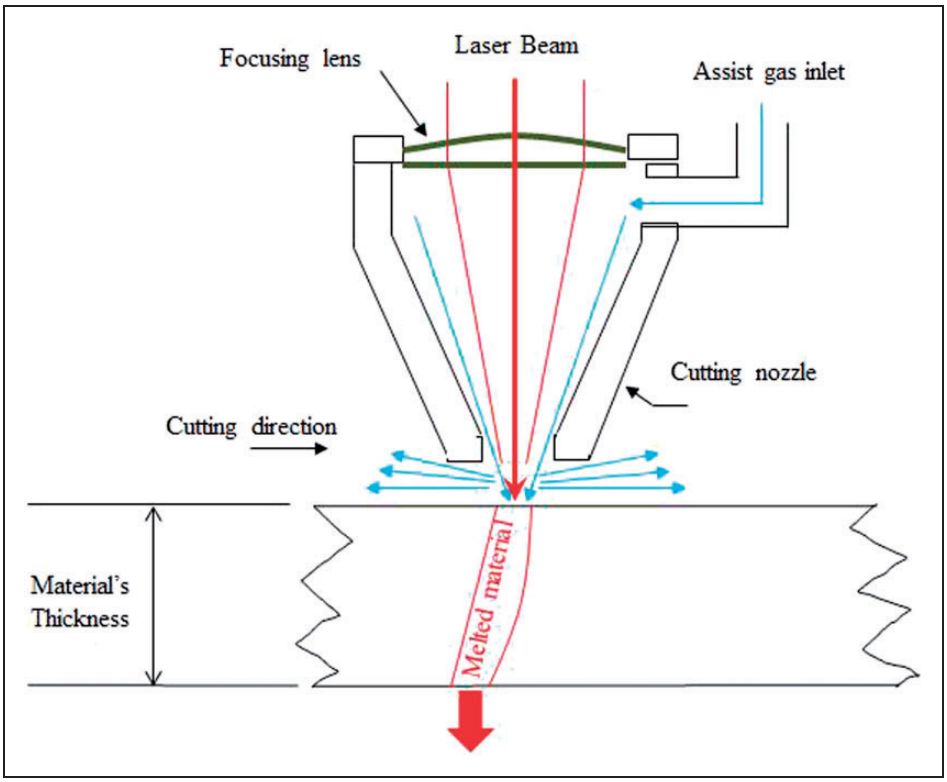

Figure 5. Laser cut nozzle system drawing.

where:

R	Lankford anisotropy values
ε_w	specimen's width true strain
ε_t	specimen's thickness true strain
ε_l	specimen's length true strain
W_o	specimen's original width
W_f	specimen's final width
L_o	specimen's original length
L_f	specimen's final length
$\overline{R}$	normal anisotropy
ΔR	planar anisotropy
R_0	Lankford value at 0°
R_{45}	Lankford value at 45°
R_{90}	Lankford value at 90°

Square blanks with sides measuring 90 mm were used for the Erichsen tests, which used a spherical 20-mm diameter punch tool, a 27-mm diameter die,

Table 3. Mechanical properties obtained by tensile tests for S_{II}, S_{IV}, and S_{VI}.

		Yield limit (MPa)		Ultimate tensile strength (MPa)		Elongation percent (80.00 mm)	
Sheet	Direction	Average	SD	Average	SD	Average	SD
II	0°	284	4	299	4	4.4	0.2
	45°	282	11	295	12	4	0.6
	90°	285	17	296	14	4.1	0.9
IV	0°	257	5	272	7	4.2	0.8
	45°	249	8	268	9	4.6	0.7
	90°	259	5	278	5	4.4	1.0
VI	0°	245	7	264	8	4	0.4
	45°	257	14	274	14	4.2	0.2
	90°	271	10	286	9	3.9	0.7

SD: Standard deviation.

and a 33-mm internal diameter blank holder. A total of 27 blanks were tested, nine for each of the three sheets. The estimated punch travel velocity was 6 mm per minute. The microhardness and the surface roughness tests both used standard equipment dedicated to that end. The specimens for both tests consisted of strips cut from the three sheets. The ones used for the microhardness tests had 20×90 mm, and those used in the surface roughness tests had 70×100 mm. The Vickers tests were realized with 50 g, 100 g, and 200 g loads for 10 s. Each sheet had five measurements taken for each of the loads. The roughness tests used an evaluation length of 4.0 mm and a sampling length of 0.8 mm. Five measurements were taken in the RD and five in the transverse direction (TD) for each sheet, making a total of 30.

The microscopy samples were polished with an MgO solution before being attacked for 120 s by hydrofluoridic acid with 1.5% concentration. The optical images were captured on an Olympus BX60M microscope with magnifications of 200×, 500×, and 1000×. Only the highest magnification images are displayed in this article. SEM images were acquired by a Jeol JSM-6510 coupled with an EDS attachment. The orientation distribution functions (ODFs) were obtained by a Rigaku Dmax 2000 diffractometer with an automatic goniometer. The radiation used was Mokα1 ($\lambda = 0.7093$ Å), with a 5° angular step and 5 s dwell time. The crystallographic planes chosen for the pole figures were (111), (200), (220), and (311).

Results and discussion

The mechanical properties of the three sheets were similar to each other with S_{II} displaying slightly higher resistance than the other two. This slight difference may be caused by small variations in the production process which were not identifiable by the realized characterizations. Overall, the results were similar to those found in a related work and in material data sheets with standard values.[9] As expected, the intense cold work diminished the ductility while increasing its yield strength and ultimate tensile strength. Table 3 shows the results for the mechanical properties of S_{II}, S_{IV}, and S_{VI}. Although S_{II} displayed higher values, the standard deviation between specimens was considerable. Each of the values displayed at Table 3 is an average of the four specimens tested for each direction.

Table 4. Average mechanical properties values separated by the specimen directions.

Angle	Yield limit (MPa) Average	Ultimate tensile strength (MPa) Average	Elongation percent (80.00 mm) Average
0°	262	278	4.2
45°	263	279	4.3
90°	272	287	4.1

In addition, if the data is put together in function of the specimen directions, no discernable differences are found either, a result which corroborates a similar study realized by Yu et al.[9] This evenness of values between different angles of a material known to display anisotropic behavior is probably related to a careful manufacturing process that aims to balance the recrystallization textures generated in the homogenization step with those accentuated in the cold rolling step in order to diminish the so called earing effect.[4] Table 4 shows the average mechanical properties values for the different sheets separated by specimen direction.

The strain hardening exponent (n) is an important factor for materials that will withstand deep drawing, since it is related to the capacity to strain harden and therefore delay localized deformation that will lead to failure. In a work dealing with an aluminum alloy dedicated to beverage can fabrication, Folle et al.[3] state that the higher the n, the higher the strength and strain absorption capability. In the same study, it can be seen that for similar reduction parameters,

Table 5. Average strain hardening exponent (n) for the three studied sheets.

		Strain hardening exponent n		
Sheet	Direction	Average	SD	$n_{average}$
II	0°	0.074	0	0.072
	45°	0.070	0	
	90°	0.073	0	
IV	0°	0.083	0	0.086
	45°	0.091	0	
	90°	0.086	0	
VI	0°	0.082	0	0.077
	45°	0.077	0	
	90°	0.073	0	

SD: standard deviation.

Table 6. Plastic strain ratios (R, ΔR, and $\overline{R}$) for the three studied sheets.

Sheet	R_{angle}		ΔR	$\overline{R}$
II	R_0	0.132	0.00596	0.438
	R_{45}	0.435		
	R_{90}	0.750		
IV	R_0	0.194	−0.0781	0.344
	R_{45}	0.383		
	R_{90}	0.417		
VI	R_0	0.235	−0.0906	0.394
	R_{45}	0.440		
	R_{90}	0.463		

Table 7. Erichsen tests results for the three sheets.

Sheet	Average punch travel in mm
II	4.42
IV	4.62
VI	4.83

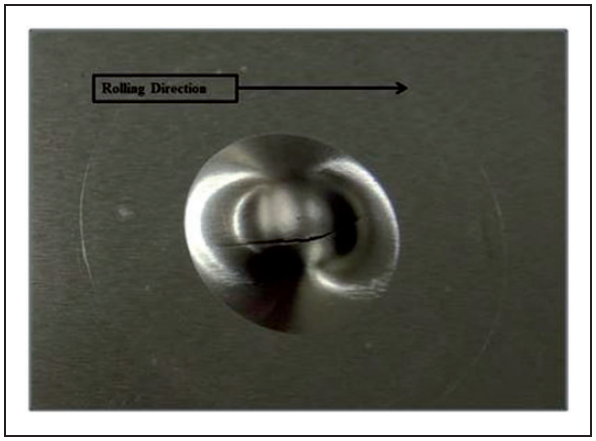

Figure 6. Erichsen test specimen displaying a fracture parallel to its rolling direction.

the drawing limit is increased as the strain hardening exponent is lowered, signifying that a higher n is desirable to stay below the maximum feasible reduction of 0.866 found by Rubio et al.[10] The values for n found for S_{II}, S_{IV}, and S_{VI} can be seen in Table 5. All had similar results, averaging 0.078. All values in Table 5 represent the average of the specimens tested in each direction. The values to the far right are the average of each sheet.

The plastic strain ratios for the three sheets can be seen in Table 6. High normal anisotropy ratios ($\overline{R}$) indicate that the material will resist deformation in the thickness direction, while low planar anisotropy values (ΔR) indicate the material will behave similarly in different strain directions, and therefore have a low earing tendency. It has been shown that plastic strain ratios can be directly correlated with earing behavior.[11] Ideal materials for deep drawing and ironing should have the lowest possible ΔR while having the highest possible $\overline{R}$, suggesting that it will have low tendency to generate ears and will resist deformation through its thickness, delaying localized strain and failure. All three sheets displayed low planar anisotropy values and relatively higher normal anisotropy values, indicating that all three are appropriate for deep drawing. Negative values for ΔR indicate a tendency to form ears at 45° in relation to the RD, which is in agreement with the deformation textures intensities acquired after cold rolling.

The Erichsen tests results can be seen in Table 7. Here again the similarities between the three sheets were evident, all failed after the punch had dislocated approximately 4 mm. All failures occurred parallel to the RD, as shown in Figure 6. It is possible that these parallel fractures have a relation to the different intermetallic compounds distributed in the Al matrix, being that the commonly found $Al_6(Fe,Mn)$ at times elongates in the RD after severe cold rolling.

The results of the microhardness Vickers tests for all three sheets can be seen in Table 8. Three different loads were used to ascertain the correct results because of the reduced material thickness. S_{II} displayed higher values as would be expected since it also had higher mechanical properties, and both have been found to be correlated.

In the previously mentioned work, Folle et al.[3] found the coefficient of friction to be the variable that most strongly influenced the ironing force, followed by the gap between the punch and the ironing dies. The coefficient of friction can be correlated with the surface roughness of the alloy and its interaction with the punch and the iron surfaces. In his work related to die wear and punch surface textures, Kang[12] mentions the importance of the differential friction ratio defined as the coefficient of friction of

Table 8. Microhardness Vickers results for the three sheets.

Load (g)	HV	S_{II}	S_{IV}	S_{VI}
200	Measurement 1	107	83	94
	Measurement 2	102	96	96
	Measurement 3	114	91	99
	Measurement 4	98	99	99
	Measurement 5	99	94	99
100	Measurement 1	101	98	96
	Measurement 2	105	95	97
	Measurement 3	106	111	93
	Measurement 4	108	106	89
	Measurement 5	105	108	92
50	Measurement 1	107	83	94
	Measurement 2	102	96	96
	Measurement 3	114	91	99
	Measurement 4	98	99	99
	Measurement 5	99	94	99
–	Average	104	93	98

Table 9. Average surface roughness (R_a) results for the three sheets.

	Roughness (R_a) μm			
Sheet	RD	TD	Average RD	Average TD
II	0.21	0.59	0.25	0.56
	0.26	0.51		
	0.27	0.59		
	0.31	0.54		
	0.19	0.54		
IV	0.27	0.44	0.21	0.45
	0.27	0.46		
	0.17	0.51		
	0.14	0.42		
	0.20	0.41		
VI	0.10	0.43	0.14	0.39
	0.10	0.35		
	0.27	0.44		
	0.10	0.37		
	0.10	0.37		

RD: rolling direction; TD: transverse direction.

the punch in relation to the alloy (μ_p) divided by the coefficient of friction of the alloy in relation to the die (μ_d) in regards to wall stresses. Both these works highlight the importance of the surface condition to the processes of deep drawing, in addition to tooling specifications and lubrication parameters. The average surface roughness (R_a) for S_{II}, S_{IV}, and S_{VI} can be seen in Table 9. Roughness values differed noticeably between the RD and the TD. Once again S_{II} displayed higher values than the other two sheets, in both directions. This can be a direct consequence of work roll root mean square roughness and the alloy surface texture anisotropy ratio and is the reason why CBS is supplied with varying degrees of frictional characteristics.[12] The wear of the cold mill work roll directly influences the surface roughness of the aluminum sheet, as more production output goes through the tendency is for the work roll to change its surface roughness characteristics. In light of that, there probably will be differences in the surface roughness of the laminated material from the first run until the time the work roll useful life is spent. The differences in the surface roughness of the studied sheets are most likely influenced by the surface condition of the work roll at the time they were produced. In their work related to surface topography and frictional characteristics of AA 3104 aluminum alloy, Saha et al.[13] mention a typical mill finish of about 35μm (R_a) for this kind of material.

Another factor that strongly influences the performance of this alloy on the production line is its crystallographic texture. Depending on which texture components have a higher intensity, different earing behaviors can occur and that may adversely affect the deep-drawing process.[2,4] Earing can cause more material to be scraped after edge trimming, and depending on its intensity, it may cause pinched or clipped off ears that will jam the ironing equipment, commonly called bodymaker.[14] The AA 3104 alloy crystallographic texture is so relevant in the subsequent manufacturing processes that its own fabrication is strictly controlled to yield a balanced texture. In the mills dedicated to CBS, fabrication parameters are tightly control to ensure that a certain intensity of Cube (Cb) texture is maintained to counterbalance the deformation textures, mainly Brass (Bs) and Copper (Cu), that develop during the cold rolling stage.[4] Another factor that points to the importance of texture and its earing correlation is the development of nonround cut edges that offer a mechanical solution to a characteristic earing tendency, leaving material available where troughs should develop and extracting more material where peaks should form.[14]

The Cube texture, {001}<100>, is typical of recrystallized face centered cubic (FCC) metals and upon strain has a tendency to ear at 0° and 90° in relation to the RD. The deformation textures Brass, {110}<112>, and Copper, {112}<111>, common in FCC metals that have gone through cold work tend to cause ears at 45° in relation to the RD. The result of a well-adjusted process with appropriate recrystallization during the inner-annealing step in addition to the correct reduction schedule in the cold mill stage is a material that will have six or eight ear with similar intensities, mimicking an isotropic material.[2] The crystallographic texture of the three studied sheets are displayed below by ODFs that follow Euler's triple angles (φ_1, Φ, and φ_2) using Bunge's notations. The ODFs below assume orthotropic symmetry and

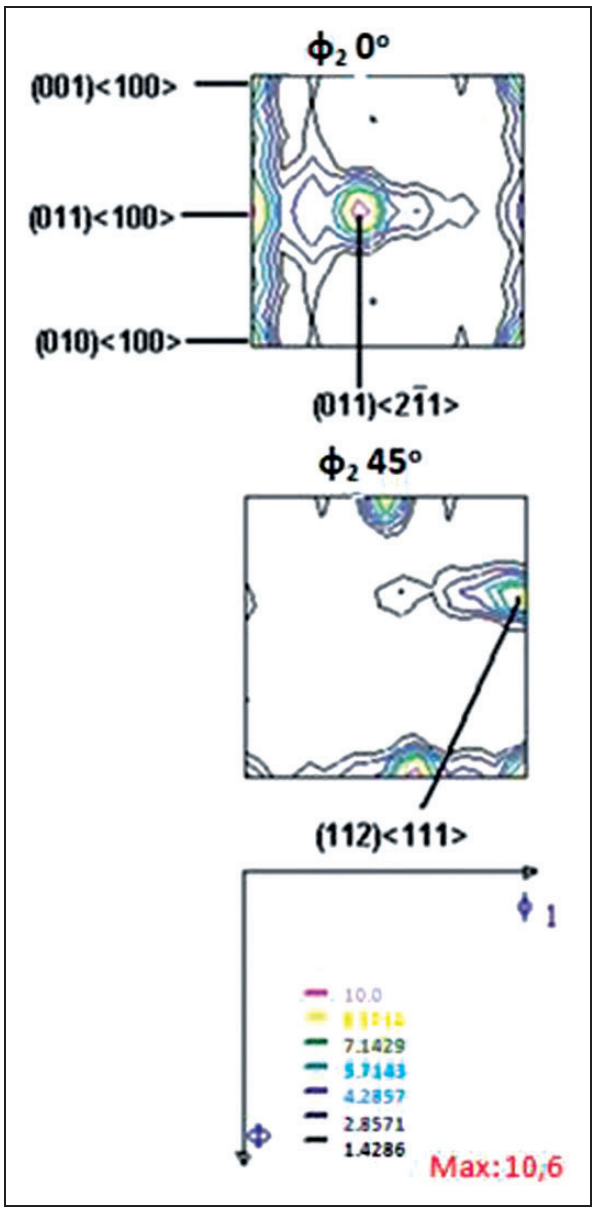

Figure 7. S_{II} orientation distribution functions (ODFs) obtained by X-ray diffraction.

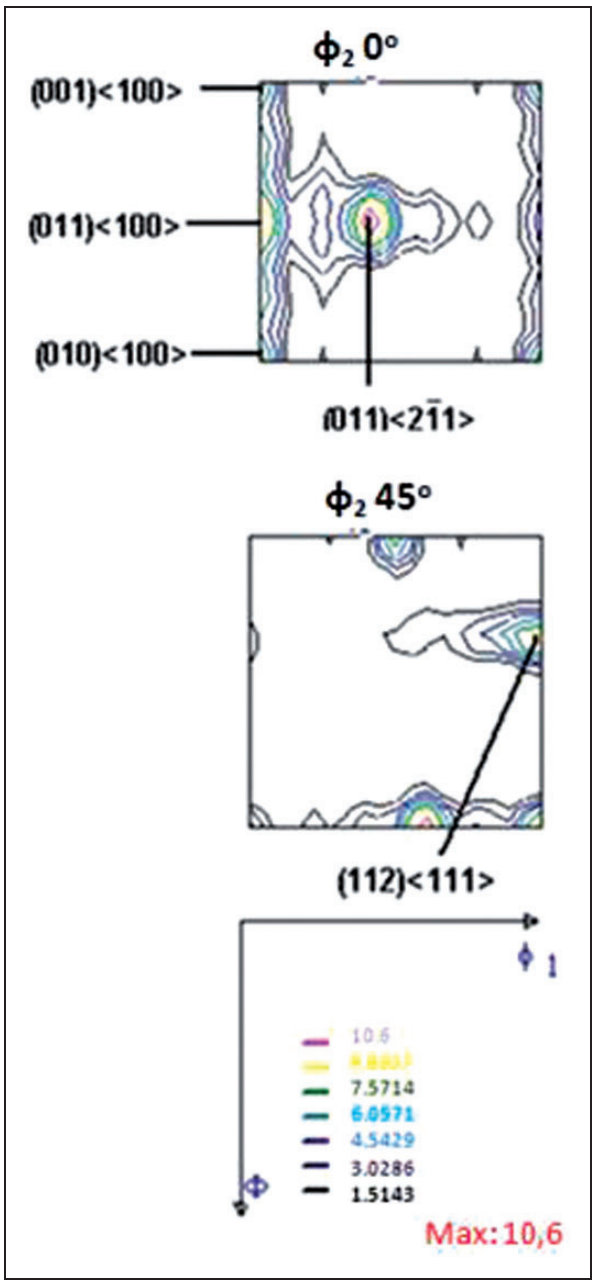

Figure 8. S_{IV} orientation distribution functions (ODFs) obtained by X-ray diffraction.

are represented by iso-intensity lines in two sections, $\varphi_2 = 0°$ and $\varphi_2 = 45°$. Figures 7 to 9 show the ODFs for S_{II}, S_{IV}, and S_{VI}, respectively. All three sheets displayed similar textures and intensities. It is possible to note on all three comparable intensities for the Cube {001}<100>, Goss {110}<001>, Brass {110}<112>, and Copper {112}<111> textures, characterizing a well-balanced texture.

The microstructure of the alloy is influenced by the direct chill casting parameters used to make the ingot, the temperature and time used in the homogenization oven, its chemical composition, in addition to the cold work which breaks up and distributes the intermetallic compounds throughout the aluminum matrix. Alexander and Greer[15] mention in a work related with intermetallic transformations of 3XXX series aluminum alloys that sheet texture and galling resistance are among the most important factors that contribute to a good performance in DWI processes. The microstructural characteristics of an alloy are thought to influence crystallographic texture after processing since the size and the distribution of intermetallic compounds or second-phase particles play an important role in recrystallization, especially for materials that have been cold worked.[9] Galling resistance is also influenced by the size and type of intermetallic compound found in the alloy and a minimum desired particle volume of 5% to 8% have been reported to aid in tooling aluminum oxide pick-up removal.[15]

The intermetallic compounds most often found in 3104 aluminum alloy used as CBS are the

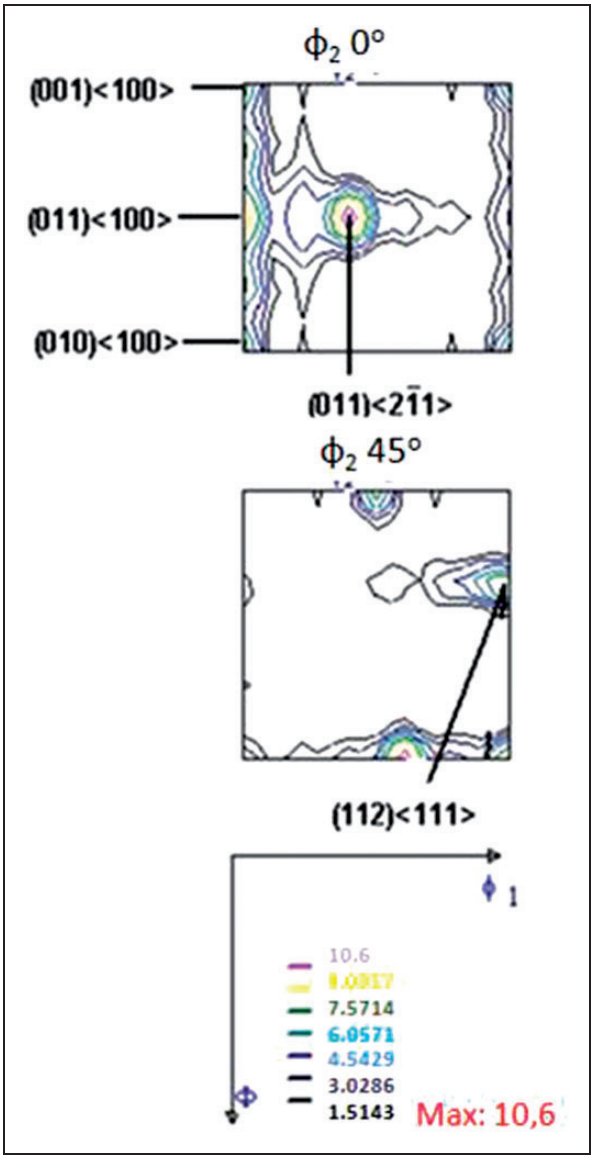

Figure 9. S_{VI} orientation distribution functions (ODFs) obtained by X-ray diffraction.

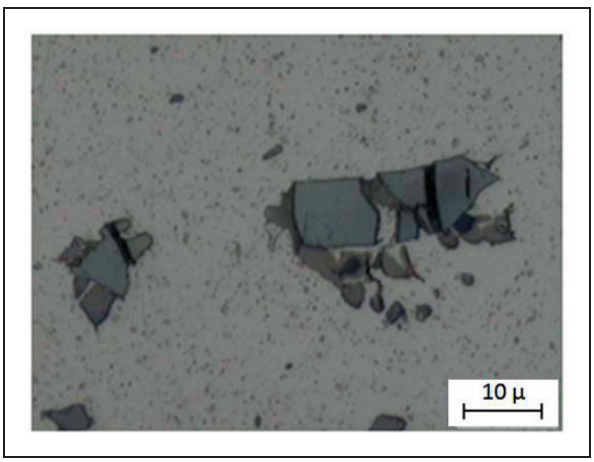

Figure 10. Optical microscopy image of S_{II}.

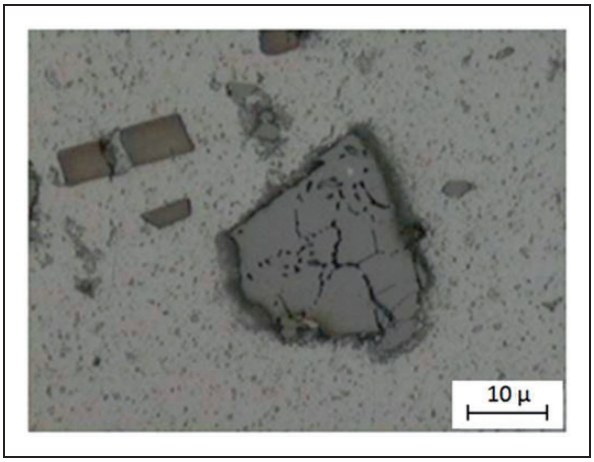

Figure 11. Optical microscopy images of S_{IV}.

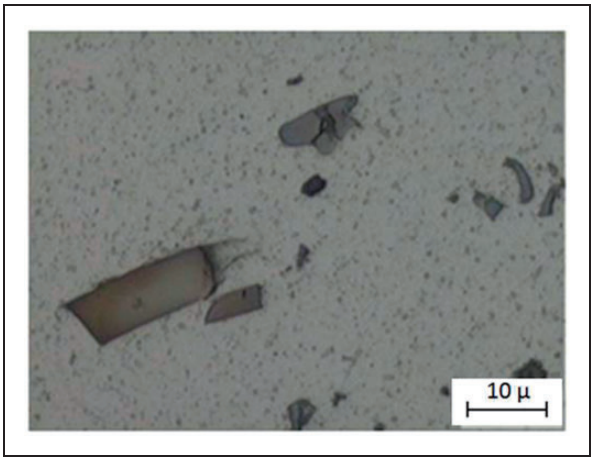

Figure 12. Optical microscopy images of S_{VI}.

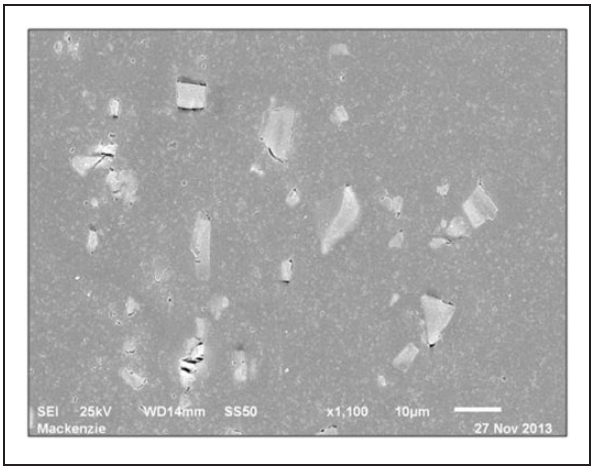

Figure 13. Scanning electron microscopy (SEM) image of S_{VI} sheet.

orthorhombic $Al_6(Fe,Mn)$ and the cubic $Al_x(Fe,Mn)_ySi$.[1,6,9,15] The transformation of the $Al_6(Fe,Mn)$ compound into the harder $Al_x(Fe,Mn)_ySi$ takes place during the homogenization

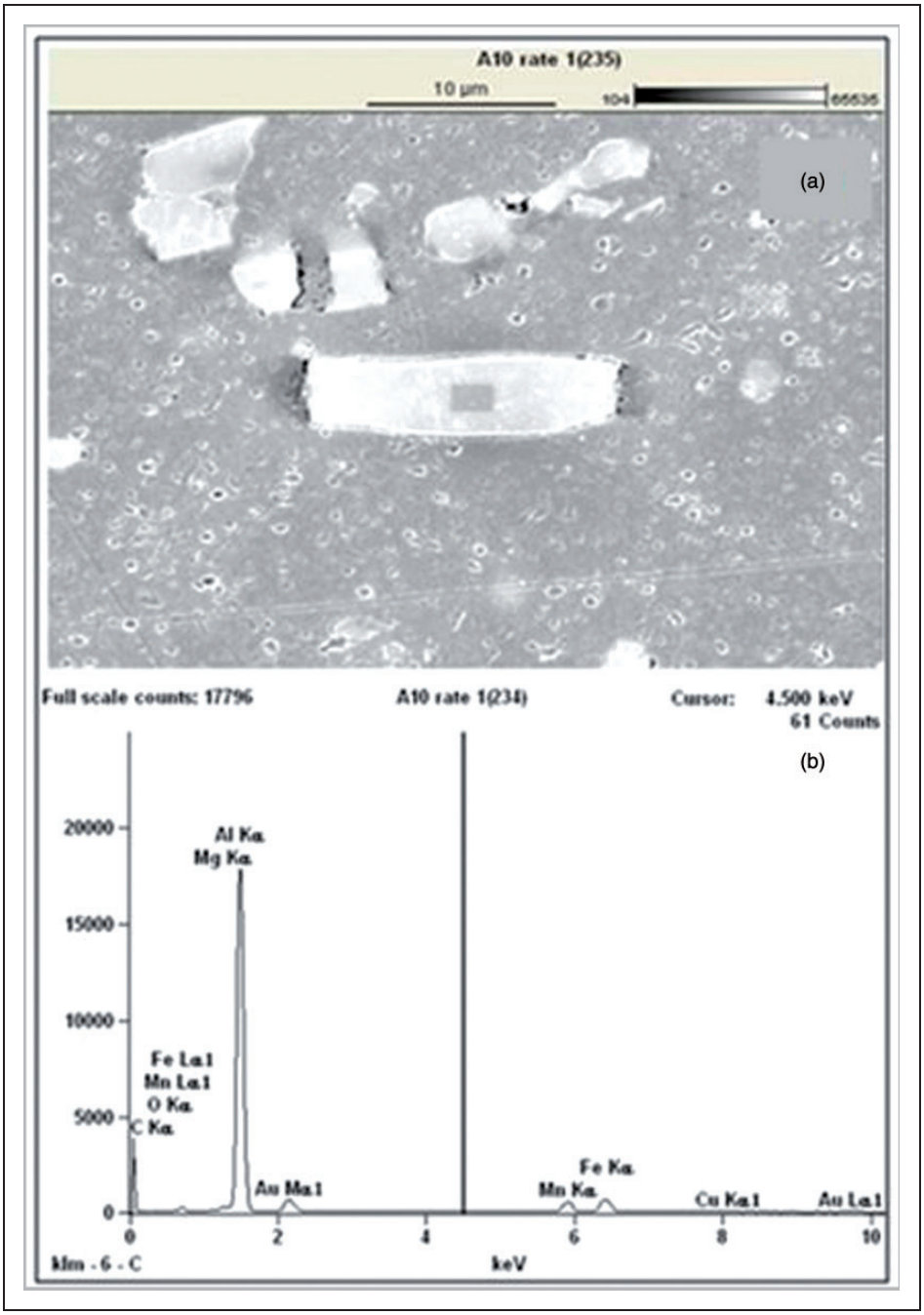

Figure 14. Scanning electron microscopy (SEM) image of S_{VI} sheet (a) evidencing intermetallic compound $Al_6(Fe,Mn)$ with respective energy dispersive spectroscopy (EDS) analysis (b).

process that precedes hot rolling and its occurrence is very important to the performance during deep drawing.[15] The images obtained for S_{II}, S_{IV}, and S_{VI} show two main types of intermetallic compounds not homogeneously spread, distinguishable by their morphology in addition to dispersoids finely distributed throughout the aluminum matrix. One type of primary particle, later confirmed to be $Al_x(Fe,Mn)$ by an EDS analysis, shows a more elongated kind of geometry. The other, with a more equiaxial morphology, had Si in its composition. The images for S_{II}, S_{IV}, and S_{VI}, with the higher magnifications (1000×) can be seen in Figures 10 to 12, respectively.

The SEM images showed the already mentioned microstructure. It is possible to distinguish some areas around the intermetallic compounds that appear to be unattached to it, probably due to the polishing process before the images were captured. In addition, the dispersoids, shown darker throughout the matrix, can be readily identified. The EDS attachment was used in the matrix and in different intermetallic compounds to qualitatively establish which elements were present in its composition. Figures 13 to 15 show images acquired from S_{VI}. The other two sheets yielded similar images and results. Figure 13 shows the microstructure with its intermetallic

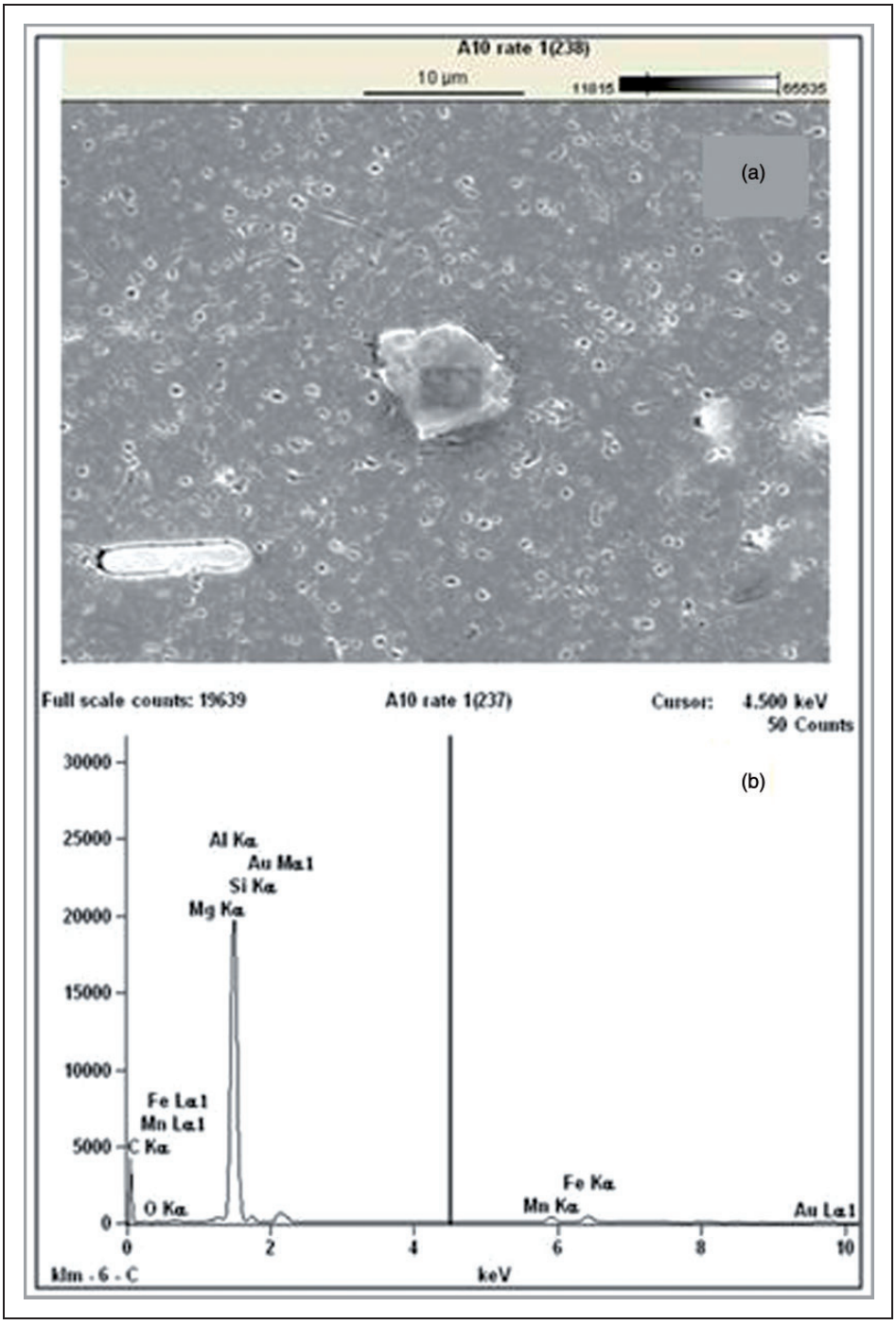

Figure 15. Scanning electron microscopy (SEM) image of S_{VI} sheet (a) evidencing intermetallic compound $Al_x(Fe,Mn)_ySi$ with respective energy dispersive spectroscopy (EDS) analysis (b).

compounds and dispersoids. Figure 14 shows the EDS of the intermetallic compound that does not have Si in its composition and the image captured during the data collection (reason why there is a darker area on the particle where the beam was incident). Figure 15 shows the other kind of compound which has a more equiaxial morphology and has Si in its composition. It is the $Al_x(Fe,Mn)_ySi$ phase that is thought to aid in aluminum oxide die cleaning if its size is between 1 and 15 µm and its volume in the matrix is appropriate.[15]

The intermetallic particles found in the present work displayed a variety of sizes, mostly ranging from 5 to 20 µm. Compounds which appear to have similar dimensions on both directions shown in the images are likely to be α-Al-(Fe,Mn)-Si. These particles are harder than the $Al_6(Fe,Mn)$ and for that reason maintain this more equiaxial morphology even after severe cold rolling. Particles that display a more elongated morphology are likely to be $Al_6(Fe,Mn)$ and assume this geometry because they break down and deform in the RD during the cold mill stage.

Conclusions

All three sheets displayed similar results for all the realized characterizations. Sheet II (S_{II}) had slightly higher mechanical properties than the other two, including a higher surface roughness, and S_{VI} showed smaller and fewer intermetallic compounds. Overall, all three appear to have the necessary elements to perform well in deep-drawing operations:

- Average yield strength of 265 MPa, average ultimate tensile strength of 281 MPa, and percent elongation of 4%;
- Strain hardening exponents averaged 0.078;
- Low planar anisotropy (ΔR), average −0.054, with relatively higher normal anisotropy ($\overline{R}$), average 0.392;
- Erichsen tests averaged 4.6 mm punch travel before failure;
- Microhardness values averaged 98 HV;
- Surface roughness Ra averaged 0.20 μm in the RD and 0.46 μm in the TD;
- A balanced crystallographic texture composed of the recrystallization Cube component {001}<100> in similar intensity as the deformation Brass {110}<112> and Copper {112}<111> components;
- A microstructure composed of nonhomogeneous dispersed intermetallic compounds and well distributed dispersoids throughout the Al matrix;
- Good size intermetallic compounds which can help in galling resistance.

The main differences between the three studied sheets can be summarized in the higher mechanical properties and surface roughness of S_{II}, which could positively influence its performance in the DWI manufacturing process and the smaller and fewer intermetallic compounds found in S_{VI} that could be detrimental to its galling resistance, making the necessity of die polishing or die changing more frequent. Although it has been stated that deep-drawing and ironing operations are strongly influenced by many factors, especially lubrication regimes, tooling frictional characteristics, and reduction progressions, it should also be noted that the properties and characteristics of the material are also very important to ensure smooth running operations.

Declaration of conflicting interests

The author(s) declared no potential conflicts of interest with respect to the research, authorship, and/or publication of this article.

Funding

The author(s) received no financial support for the research, authorship, and/or publication of this article.

References

1. Vasudevan AK and Doherty RD. *Aluminum alloys – contemporary research and applications*. San Diego: Academic Press, 1989.
2. Engler O and Hirsch J. Polycristal-plasticity simulation of six and eight ears in deep-drawn aluminum cups. *Mater Sci Eng A* 2007; 453: 640–651.
3. Folle F, Netto S and Schaefer L. Analysis of the manufacturing process of beverage cans using aluminum alloy. *J Mater Process Technol* 2008; 205: 247–352.
4. Engler O. Control texture and earing in aluminum alloy AA 3105 sheet for packaging applications. *Mater Sci Eng A* 2012; 538: 69–80.
5. Korhonen A. On the work hardening of AA 3104-H19 aluminum alloy. *J Mater Eng Perform* 2013; 22: 505–511.
6. Totten GE and Mackenzie SD. *Handbook of aluminum – volume 1: physical metallurgy and processes*. Boca Raton, FL: CRC Press, 2003.
7. ASM International Handbook. Volume 2 Properties and selection: nonferrous alloys and special purpose material [CD-ROM], 1992.
8. ASM International Handbook. Volume 8 Mechanical testing and evaluation [CD-ROM], 2000.
9. Yu TM, Brooks CR and Goodrich S. The effect of cold working and annealing practice on earing in 3104 Al alloy sheet. *Mater Char* 1993; 30: 251–259.
10. Rubio EM, Gonzalves C, Marcos M, et al. Energetic analysis of tube drawing processes with fixed plug by upper bound method. *J Mater Process Technol* 2006; 177: 175–178.
11. Ren B, Zhong L and Morris JG. Correlation between the preferred grain orientation and deep-drawing behavior of AA 3104 and AA 5052 aluminum alloy sheets. *Scr Metall Mater* 1994; 31: 387–392.
12. Kang K. Impact of die wear and punch surface textures on aluminum can wall. *Wear* 2009; 266: 1044–1049.
13. Saha PK, Wilson WRD and Timsit RS. Influence of surface topography on the frictional characteristics of 3104 aluminum ally sheet. *Wear* 1996; 197: 123–129.
14. Engler O, Merterns N and Dam P. Texture based design of a convoluted cut-edge for earing free cans. *J Mater Process Technol* 2011; 211: 1278–1284.
15. Alexander DTL and Greer AL. Solid-state intermetallic phase transformation in 3XXX aluminum alloys. *Acta Mater* 2002; 50: 2571–2583.